Simulation of InP-based monolithically integrated PIN-HEMT front-end optical receiver

Sheng Xie[*], Chao Chen, Jiantao Bian

(Department of Physics, Xiamen University, 361005, P.R.China)

Abstrcat

Model is developed for the dc I-V characteristics and microwave small-signal parameters of the InP-based $In_{0.52}Al_{0.28}As/In_{0.65}Ga_{0.35}As$ HEMT's based on physical principles, and the effect of the extrinsic source and drain resistances has also been included. Using the parameters obtained by this model and the small-signal model of PIN detector, we simulated the transimpedance configurations with an inverter and a cascode input circuit of monolithically integrated PIN-HEMT front-end optical receiver. The results indicate that the cascode input stage can realize a smaller input capacitance than the inverter-type, so it has a wider bandwidth. In order to operate in 2.5Gb/s transmission system, the cascode input stage is applied and the parameters are optimized. The simulations reveal that the transimpedance gain is larger than 63.2dB Ω and the sensitivity is 30dBm when the bit rate is 2.5Gb/s. The results obtained in this paper provide a guideline for the fabrication of PIN-HEMT optical receiver.

Keyword: optical receiver; HEMT; PIN; OEIC; monolithic

1. Introduction

The rapid increase of data rates in fiber-optic communication system requires high-sensitivity optical receiver capable of operating at high speeds. In order to achieve this goal, an alternative way is to minimize the parasitics of a front-end optical receiver. Considering state-of-the-art integration, one attractive approach is to monolithically integrate the photodetector (PD) with the active electrical devices for amplification and signal processing on the same substrate. As we know, the materials grown lattice matched to InP substrate are well-suited to long-wavelength (1.3~1.55 μ m) communications of silica optical fibers. Meanwhile, InP also shows good electronic properties such as high peak electron velocity, high breakdown field and high thermal conductivity. Therefore, InP-based optoelectronic devices have been considerably interested in the past decades. However, due to gate-semiconductor interfacial problems, the metal-insulator-semiconductor (MIS) and metal-semiconductor (MES) FET's do not feasible on InP, this makes

HEMT's become the best choice. Furthermore, as the progress of electrical devices is considered, HEMT's are the fast three-end devices at the present time[1]. Meanwhile, it has the virtues of low noise, high output power and power-added efficiency[2-4]. On the other hand, in comparison with avalanche photodiodes (APDs) and mental-semiconductor-mental (MSM) PDs, PIN PD has the virtues of low leakage current and high sensitivity. Hence, the integration scheme of a PIN PD and a HEMT-based amplifier, as shown in Fig. 1, is one of the most potential candidates in the long-haul high-speed
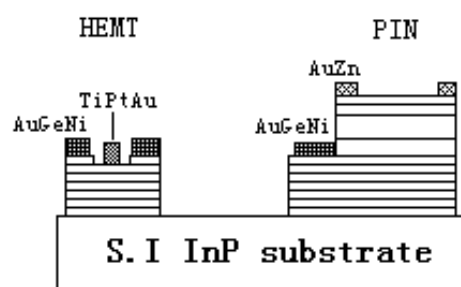

Fig. 1. Cross-sectional view of PIN-HEMT integration scheme

[*] xie_sheng96@163.com; phone: +86-592-218-4426; fax:+86-592-218-9426

transmission networks[5-7]. For exploiting the potential performances of PIN-HEMT front-end optical receiver, developing simple yet accurate device and circuit models are required.

In this paper, an analytical model of InP-based $In_{0.52}Al_{0.28}As/In_{0.65}Ga_{0.35}As$ HEMT's is proposed based on physical principles in Sec. 2, which includes the effect of the extrinsic source and drain resistances. In Sec. 3 we analyze the gain and the –3dB frequency of a transimpedance optical receiver, and calculate the input noise current for determining the effect of noise sources and parasitic capacitance on the input stage. In order to operate in 2.5Gb/s transmission networks, the parameters are optimized. Finally, in Sec. 4, we present the simulated results of the front-end optical receiver with a cascode input stage.

2. Analytical model of HEMT

The analytical model presented in this paper is based on the following assumptions. First of all, the gradual channel approximation (GCA) is valid in the portion of channel where electron velocity is smaller than the saturation velocity. Second, once the velocity saturation occurs near the drain edge of the channel, further increase in the drain current is only due to channel length modulation. Third, the gate current is neglected in order to make the model simple. This assumption is valid to voltages below the turn-on voltage for the gate current. Forth, the relation between the electric field and the electron velocity is given by a modified two-piece approximation. Finally, the parasitic MESFET is neglected since the circuits operate at $V_g=0$.

According to the charge control mode, the sheet charge density $n_s(x)$ in the two-dimension electron gas (2DEG) above the threshold can be expressed as follows[8]:

$$n_s(x) = \frac{\varepsilon_s}{qd_t}(V_{GT} - V_c(x)) \tag{1}$$

Where ε_s is the dielectric permittivity of $In_{0.52}Al_{0.48}As$ (hereafter referred to as InAlAs) layer, d_t is the total thickness from the gate surface to the top heterojunction, $V_{GT} = V_{GS} - V_T$, V_T is the threshold voltage, V(x) is the 2DEG potential at a distance x from the source edge of the channel. For the uniform doping InAlAs layer, V_T is given by

$$V_T = \phi_M - \frac{\Delta E_C}{q} - \frac{qN_d d_d^2}{\varepsilon_s} \tag{2}$$

Where $\phi_M = 0.655V$ is the barrier height of the Schottky gate, if Ti/Pt/Au is applied[9], ΔE_C is the conduction band discontinuity at heterojunction, N_d is the doping concentration in n-InAlAs layer, d_d is the doped InAlAs layer thickness.

At the common conditions, the diffusion current is much less than the drift current, and can be neglected. Therefore, the current-voltage relation is expressed as follows:

$$I_{ds} = qn_s(x)v(x)Z \tag{3}$$

Where Z is the gate width, q is the electronic charge, $v(x)$ is the electron drift velocity. In this paper, the modified

two-piece approximation[10] is applied.

$$v(x) = \frac{\mu_n E(x)}{1 + E(x)/2E_C} \qquad\qquad E \leq 2E_C = 2v_{sat}/\mu_n \qquad\qquad (4a)$$

$$v(x) = v_{sat} \qquad\qquad E \geq 2E_C = 2v_{sat}/\mu_n \qquad\qquad (4b)$$

Where μ_n is the low-field mobility, v_{sat} is the electron saturation velocity, E_C is the critical field. Taking the field distribution and the boundary conditions of intrinsic device into account, and integrating from the source $x = 0$ to the drain $x = L$. The drain current I_{DS}, in the linear region, is found to be expressed as

$$I_{DSL} = \beta \frac{2V_{GT}V_{DS} - V_{DS}^2}{2V_L + V_{DS}} \qquad\qquad (5)$$

where $\beta = \frac{\varepsilon_s Z v_{sat}}{d_t}$, $V_L = E_C L$, L is the gate length.

At $V_{DS} = V_{DSAT}$, the electron drift velocity at the drain edge of the channel is saturated at v_{sat}. Here, one can obtained

$$V_{DSAT} = \frac{2V_{GT}V_L}{V_{GT} + V_L} \quad \text{and} \qquad\qquad (6)$$

$$I_{DSAT} = \beta \frac{V_{GT}^2}{V_{GT} + 2V_L} \qquad\qquad (7)$$

When V_{DS} becomes larger than V_{DSAT}, the point of saturation moves closer to the source. In this case, the channel can be divided into two regions. The drain current in the saturation region I_{DSS} can be obtained from Eq. (7) by replacing V_L with $V_L - V_{\Delta L} = E_C(L - \Delta L)$, where ΔL is the saturation length of the channel.

$$I_{DSAT} = \beta \frac{V_{GT}^2}{V_{GT} + 2(V_L - V_{\Delta L})} \qquad\qquad (8)$$

According to the derivation of ΔL by Byung-Jong Moon[10], the drain current in the saturation region can be expressed

$$I_{DSS} = I_{DSAT} \left[1 + \frac{2V_\zeta}{V_{GT} + 2V_L} In \left\{ 1 + \frac{(V_{DS} - V_{DSAT})(V_{GT} + 2V_L)^2}{8V_\zeta(V_{GT} + V_L)V_L} \right\} \right] \qquad\qquad (9)$$

where $V_\lambda = E_C \zeta$, $\zeta = \sqrt{d_t d_s}$, d_s is the effective distance of the 2DEG from the gate at saturation region[11].

When take the effect of the extrinsic source and drain resistances R_S and R_D into account, the boundary conditions are given by

$$V_{DS} = V_{ds} - I_{DS}(R_S + R_D) \tag{10a}$$

$$V_{GS} = V_{gs} - I_{DS}R_S \tag{10b}$$

Using the above boundary conditions, and integrating Eq. (3) again, one can obtain the extrinsic drain current in the linear and saturation region.

The device transconductance g_m and output conductance g_d are defined as

$$g_m = \frac{dI_{ds}}{dV_{gs}}\bigg|_{V_{ds}=cons\tan t} \quad \text{and} \quad g_d = \frac{dI_{ds}}{dV_{ds}}\bigg|_{V_{gs}=cons\tan t}$$

In the saturation region, the obtained expressions for g_{ms} and g_{ds} are

$$g_{ms} = I_{DSS}\left(\frac{2 + 4V_L/V_{GT}}{V_{GT} + 2V_L}\right) + I_{DSAT}\frac{2V_\zeta V_{GT} - (V_{GT} + V_L)^2}{(V_{GT} + 2V_L)(V_{GT} + V_L)^2} \tag{11}$$

$$g_{ds} = \left[\beta\frac{V_{GT}^2}{(V_{GT} + 2V_L)^2}\frac{2V_\zeta}{(V_{DS} - V_{DSAT})}\right] \tag{12}$$

Considering the effect of the source and drain resistances, the extrinsic transconductance and drain conductance are given as follows:

$$g_{mse} = \frac{g_{ms}}{1 + g_{ms}R_S + g_d(R_S + R_D)} \tag{13}$$

$$g_{dse} = \frac{g_{ds}}{1 + g_{ms}R_S + g_d(R_S + R_D)} \tag{14}$$

According to the charge distributive approach under quasi-static approximation proposed by M. Nawaz[12], the gate charge of HEMT's operated at saturation is given

$$Q_{Gsat} = -Q_t + (Q_{g1} + Q_{g2}) \tag{15}$$

Where $Q_t = qZLN_d d_d$, Q_{g1} and Q_{g2} are the charge contribution in the linear and saturation region, respectively.

Subsequently, the gate-source capacitance and the gate-drain capacitance can be expressed

$$C_{GS} = -\frac{dQ_G}{dV_{GS}}\bigg|_{V_{DS}=cons\tan t} = -\frac{Z\varepsilon_s}{d_t E_C}\left[\frac{4V_{GT}V_L - 2V_{DS}V_L}{(2V_{GT}-V_{DS})} - \right.$$

$$\left. \frac{2(V_{DS}^3/12 + 2V_{GT}^2 V_L + 2V_{DS}^2 V_L/3 - 2V_{GT}V_{DS}V_L)}{(2V_{GT}-V_{DS})^2}\right] - \frac{W\Delta L\varepsilon_s}{d_t}\left(1 - \frac{V_{GT}+4V_L}{(V_{GT}+2V_L)^2}\right)$$

(16)

$$C_{GD} = -\frac{dQ_G}{dV_{GD}}\bigg|_{V_{GS}=cons\tan t} = -\frac{Z\varepsilon_s}{d_t E_C}\left[\frac{V_{DS}^2/4 + 4V_{DS}V_L - 2V_{GT}V_L}{(2V_{GT}-V_{DS})} + \right.$$

$$\left. \frac{(V_{DS}^3/12 + 2V_{GT}^2 V_L + 2V_{DS}^2 V_L/3 - 2V_{GT}V_{DS}V_L)}{(2V_{GT}-V_{DS})^2}\right] - \frac{W\varepsilon_s}{d_t}(V_{GT}-V_{DSAT})\frac{\zeta}{\alpha V_\zeta + V_{DS} - V_{DSAT}}$$

(17)

Where $\alpha = \dfrac{8(V_{GT}+V_L)V_L}{(V_{GT}+2V_L)^2}$

3. Performance analyses of the front-end optical receiver

As a key element, the front-end decides the whole performances of optical receiver. Hence, it must have enough bandwidth, enough gain and low noise in the realistic optical transmission systems. Because of the virtues of wider dynamic range, small waveform distortion, and steady circuit performance, the transimpedance circuit configuration has been extensively employed in the front-end optical receiver. Fig. 2 illustrates the typical circuit diagram of a transimpedance optical receiver.
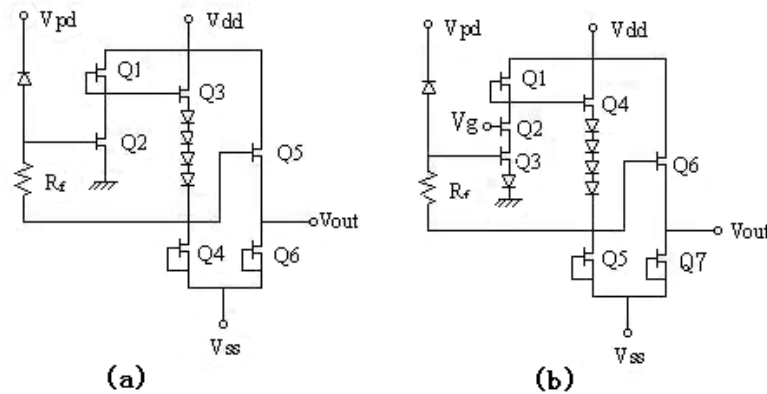

Fig. 2. Circuit diagrams of monolithic optical receiver. (a) An inverter-type optical receiver.

(b) An optical receiver with a cascode amplifier

If the effect of buffer stage is neglected, the gain of a transimpedance amplifier is represented by[13]

$$Z_t = \frac{V_{out}}{I_{in}} = \frac{R_o - AR_f}{1 + A + j2\pi f C_{in}(R_f + R_o)}$$

（18）

Where V_{out} is the output voltage amplitude, I_{in} is the photocurrent produced by the PD, R_f is the feedback

resistance, R_o is the output impedance of the source follower circuit: HEMT's Q_3 and Q_4 in Fig. 2(a), C_{in} and A are the total input capacitance and the open-loop gain of the circuit, respectively. C_{in} can be estimated by

$$C_{in} = C_{pd} + C_{FET} = C_{pd} + C_{gs2} + C_{gd2}(1 + A_2) \qquad (19a)$$

Where C_{pd} is the capacitance of the PIN PD, C_{gs2}, C_{gd2}, and A_2 are, respectively, the gate-source capacitance, the gate-drain capacitance, and the gain of HEMT Q_2. Constant A_2 is given by $A_2 = g_{m2}\dfrac{r_{ds1}r_{ds2}}{r_{ds1}+r_{ds2}}$.

Where g_{m2} is the extrinsic transconductance of HEMT Q_2, $r_{ds1} = 1/g_{dse1}$ and $r_{ds2} = 1/g_{dse2}$ are the output resistances of HEMT's Q_1 and Q_2.

For the case of cascode input stage in fig. 2(b), the gain of the common source amplifier HEMT Q_3 can be made almost unity by choosing the same transconductance value for Q_2 and Q_3. Consequence, C_{in} can be minimized to

$$C_{in} = C_{pd} + C_{FET} = C_{pd} + C_{gs} + 2C_{gd} \qquad (19b)$$

Additionally, the open-loop gain A of an inverter input stage optical receiver is given by

$$A = A_2 \times A_4 = g_{m2}\frac{r_{ds1}r_{ds2}}{r_{ds1}+r_{ds2}} \times \frac{g_{m3}\dfrac{r_{ds3}r_{ds4}}{r_{ds3}+r_{ds4}}}{1 + g_{m3}\dfrac{r_{ds3}r_{ds4}}{r_{ds3}+r_{ds4}}} \qquad (20)$$

Where g_{m3} is the extrinsic transconductance of Q_3, r_{ds3} and r_{ds4} are the output resistances of HEMT's Q_3 and Q_4.

The –3dB frequency of the front-end optical receiver is given by

$$f_{-3dB} = \frac{1+A}{2\pi C_{in}(R_f + R_o)} \qquad (21)$$

The noise performance of the monolithic integration optical receiver is usually described by the total mean square noise current[14] $<i_{tot}^2>$, which is equal to the sum of the shot noise due to the leakage current in the HEMT's gate and the detector $<i_s^2>$, the Johnson noise in the feedback resistor $<i_J^2>$, the channel noise $<i_{ch}^2>$ and the $1/f$ noise $<i_f^2>$, that is

$$<i_{tot}^2> = <i_s^2> + <i_J^2> + <i_{ch}^2> + <i_f^2> \qquad (22)$$

These noises can be estimated respectively as follows

$$<i_s^2> = 2q(I_D + I_{GS})I_2 B \qquad (23a)$$

$$< i_J^2 >= \frac{4kTI_2B}{R_F} \tag{19b}$$

$$< i_{ch}^2 >= \frac{4kT\Gamma(2\pi C_{in})^2 I_3 B^3}{g_{mse}} \tag{19c}$$

$$< i_f^2 >= \frac{8kT\Gamma(2\pi C_{in})^2 f_c I_f B^2}{g_{mse}} \tag{23d}$$

Where k is the Boltzmann's constant, q is the electronic charge, T is the absolute temperature, B is the data bit rate, I_D is the PIN PD dark current, I_{GS} is the gate leakage current, Γ is the noise figure, f_c is the $1/f$ noise corner frequency, I_2, I_3 and I_f are effective receiver bandwidth integrals which depend on the transfer function of the circuit and the input and output waveforms. Assuming a raised cosine output pulse response of the receiver for a rectangular input pulse shape, and a non-return-to-zero (NRZ) data format, it can be shown that $I_f \approx 0.12$[15], I_2=0.564, I_3=0.0868[16]

Assuming Gaussian noise statistics, the average detectable power at a certain bit-error-rate (BER) is given by

$$< P >= (Qhc/\eta q\lambda)\sqrt{< i_{tot}^2 >} \tag{24}$$

Where h is Planck's constant, c is the speed of light in vacuum, λ is the wavelength of the incident, η is the quantum efficiency of PD, and Q is a parameter related to the signal-to-noise ratio (which is almost 6 at a BER of 10^{-9}). In the following simulation, $\lambda = 1.3um$ and BER=10^{-9} are assumed.

Base on the above analyses, we can conclude that a smaller input capacitance and a large open-loop gain will produce a wider bandwidth and a larger transimpedance gain. Moreover, this can also improve the sensitivity. In addition, when the bandwidth is assured, the sensitivity can be further improved by increasing the feedback resistance.

In order to operate in 2.5Gb/s transmission system, the geometrical parameters influencing the performances have been optimized, and the optimum values are shown in table. 1.

Table 1 the parameters of HEMT

L=1 μ m	R_S=20 Ω	v_{sat}=1.55×10^7cm/s
Z=50 μ m	R_D=25 Ω	ε_s=12.45 ε_0
d_d=5nm	N_d=2×10^{18}cm^{-3}	ΔE_C=0.53eV
d_b =20nm	μ_n=13900cm^2/V·s	V_{gs}=0V
d_i=3nm	Φ_M=0.655V	V_{ds}=2.5V

4. Results

The physical and geometrical parameters of HEMT's used in the simulation are presented in table 1. Additionally, the main parameters of the PIN PD are: Φ_{pd}=30 μ m, W_{pd}=3.0 μ m, N_{pd}=5×10^{15}cm^{-3}. Using the calculated results

obtained in Sec. 2 and equations (18) (21) (22) (24) in Sec. 3, we simulate numerically the performances of the PIN-HEMT front-end optical receiver. Fig. 3 shows the relation between the –3dB frequency of the font-end receiver and the feedback resistance. It implies that the –3dB frequency decreases as the feedback resistance increases. In order to operate in 2.5Gb/s transmission systems, the cascode input stage should be adopted, and the feedback resistance must be smaller than 2.2K. However, as we know from Eq. (18), this is contrary to improving the gain of the front-end receiver. Hence, there must be a trade-off between bandwidth and sensitivity, in the following simulation, R_f=2K is assumed.
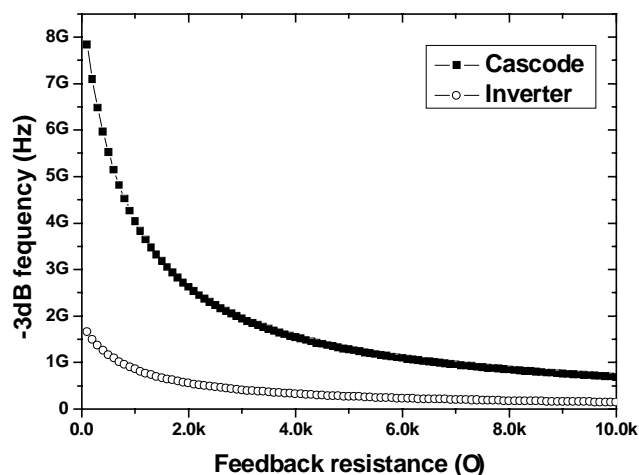
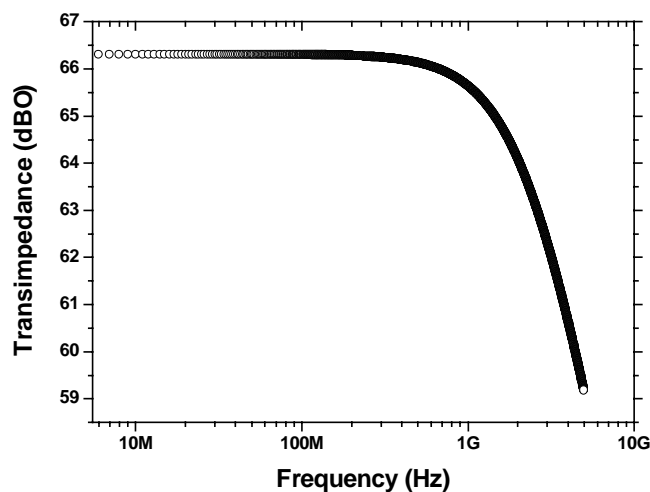Fig. 3. The dependence of –3dB frequency on the feedback resistances

Fig. 4. Frequency response of the optical receiver with a cascode input stage

The frequency characteristic of the front-end optical receiver is presented in Fig. 4. it shows that the transimpedance

gain, which is defined as $20\log(V_{out}/I_{in})$, is larger than 63.2dBΩ when the front-end receiver operated in 2.5Gb/s transmission systems.

Fig. 5 is the noise current contribution as a function of the bit rate B. It can be observed that the noise current is contributed primarily by Johnson noise in the feedback resistor $<i_J^2>$ at the low frequency. But the channel

noise $<i_{ch}^2>$, which is proportional with B^3, is the dominant contribution as the bit rate increases. Because I_{GS} and
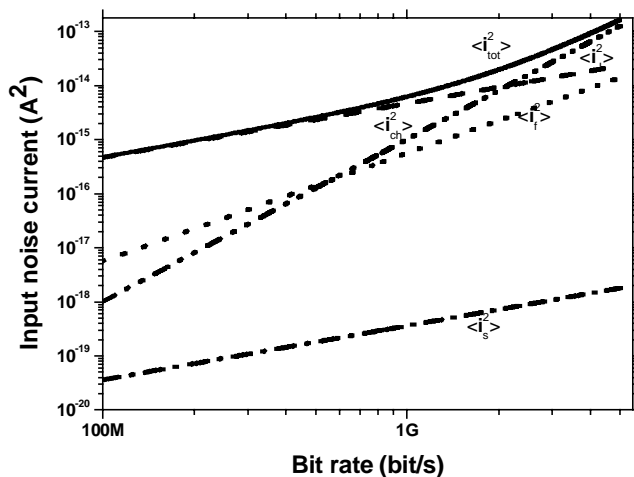

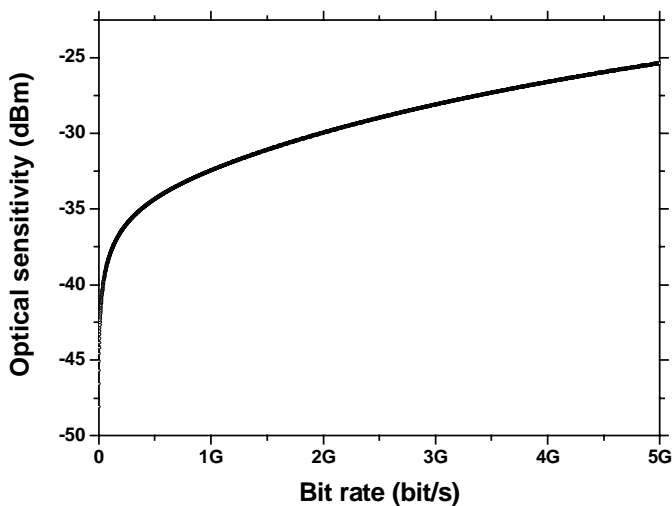Fig. 5. Bit rate dependence of Noise source

Fig. 6. Optical sensitivity versus the bit rate

I_D are taken to be in the nA range, the shot noise $< i_s^2 >$ of PIN PD and HEMT's can be neglected.

The dependence of the sensitivity on the bit rate obtained by Eq. (24), which depicts the relation between the equivalent input noise current and the sensitivity, is shown in Fig. 6. For B=2.5Gb/s, the optical receiver shows an excellent optical sensitivity (–30dBm).

5. Conclusions

We derived the static and dynamic model of InP-based $In_{0.52}Al_{0.28}As/In_{0.65}Ga_{0.35}As$ HEMT's based on physical principles. Using the results obtained by this model and the small-signal model of PIN PD, We analyzed the relations between –3dB frequency and the feedback resistance for the transimpedance circuits with an inverter and a cascode input stage, respectively. In order to operate in 2.5Gb/s transmission networks, the cascode input stage was adopted and the parameters influencing the performances were optimized. Subsequently, the transimpdedance gain and sensitivity were calculated. The results revealed that the transimpedance gain was larger than 63.2dB Ω and the sensitivity exceeded 30dBm when B=2.5Gb/s. The results obtained in this paper provide a guideline for the fabrication of PIN-HEMT optical receiver.

References

1. L.D.Ngyyen, A.S.Brown, M.A.Thompson et al., 50-nm-self-aligned-gate pseudomorphic AlInAs/GaInAs high electron mobility transistor, IEEE Trans. Electron Device, 1992, 39(9): 2007-2014.

2. T.Hwang, P.Chye, P.Gregory, super low noise pseudomorphic InGaAs channel InP HEMT's, Electron. Lett., 1993, 29(1):10-11.

3. Chen Y.C., Ingram D.L., Lai R. et al., A 95-GHz InP HEMT MMIC amplifier with 427-mW power output. IEEE Microwave and guided wave letters, 1998, 8(11): 399-401.

4. R.Grundbacher, R.Lai, M.Nishimoto et al., Pseudomorphic InP HEMT's with dry-etched source vias having 190mW output power and 40% PAE at V-band, IEEE electron device letters, 1999, 20(10): 517-519.

5. K.Takahata, Y.Muramoto, H.Fukano et al., 46.5GHz-bandwidth monolithic receiver OEIC consisting of a waveguide p-i-n photodiode and a HEMT distributed preamplifier, IEEE photon. Technol. Lett., 1998, 10(8):1150-1152.

6. N.Shimizu, K.Murata, A.Hirano et al., 40-Gbit/s monolithic digital OEIC composed of a uni-traveling-carrier photodiode and InP HEMTs, Lasers and Electro-Optics, 2000, (CLEO 2000) Conference on, 2000: 382.

7. H.G. Bach, W. Schlaak, G.G. Mekonnen, et al., 50GHz Photoreceiver Modules for RZ and NRZ Modulation Format Comprising InP-OEICs, Proc.27th Eur. Conf. on Opt. Comm. (ECOC'01-Amsterdam), 560-561.

8. T.J.Drummond, H.Morkoc, L.Lee et al., Model for modulation doped field effect transistor. IEEE electron device letters, 1982, 3(11): 338-341.

9. Larry P.Sadwick, C.W.Kim, Kin L.Tan et al., Schottky barrier heights of n-type and p-type $Al_{0.48}In_{0.52}As$, IEEE electron device letters, 1991, 12(11): 626-628.

10. B.J.Moon, Y.H.Byun, K.Lee et al., New continuous heterostructure field-effect-transistor model and unified parameter extraction technique, IEEE Trans. Electron devices, 1990, 37(4): 908-919.

11. Nandita Dasgupta and Amitava Dasgupta, A new SPICE MOSFET level 3-like model of HEMT's for circuit

simulation, IEEE transactions on electron devices, 1998, 45(7): 1494-1500.

12. M.Nawaz, Geok I. Ng., A new CAD oriented charge conserving capacitance model for HEMTs, Microelectronic engineering, 1998, 43-44:619-626.

13. Junichi Yoshida, Yuji Akahori, Mutsuo Ikeda et al., Sensitivity limits of long-wavelength monolithically integrated p-i-n JFET photoreceivers, Journal of lightwave technology, 1996, 14(5): 770-779.

14. J.J.Morikuni, A.Dharchoudhury, Y. Leblebici et al., Improvement to the standard theory for photoreceiver noise, Journal of lightwave technology, 1994, 12(4): 1174-1184.

15. D.C.W.Lo, S.R.Forrest, Performance of $In_{0.53}Ga_{0.48}As$ and InP junction field-effect transistors for optoelectronic integrated circuits, Journal of lightwave technology, 1989, 7(6): 957-965.

16. Zhang Minde, Sun Xiaohan. Fiber-optic communication: Principles and systems (second edition), Southeast University Press, Nanjing, 2001: 228.